JOURNAL OF PROPULSION AND POWER
Vol. 12, No. 2, March–April 1996

Flow Characteristics in Boundary-Layer Bleed Slots with Plenum

A. Hamed,* J. J. Yeuan,† and Y. D. Jun‡
University of Cincinnati, Cincinnati, Ohio 45221

Numerical simulations were conducted to investigate the performance characteristics of bleed through a normal slot and its effect on the turbulent boundary-layer development under zero and strong adverse pressure gradient caused by an incident oblique shock. The solution to the compressible Navier–Stokes and k-ϵ equations was obtained in a domain that includes the regions inside the bleed slot and plenum in addition to the external flow. The computational results demonstrate the interactions between the plenum, and bleed flow and the effect of incident shock on the boundary-layer development downstream. The computed results are compared with the experimentally measured bleed mass flow and the pitot and static pressure distribution inside the slot. The computations predicted the measured increase in bleed mass flow with incident shock, and agreed with the measured bleed slot pressure fields, except in the regions of experimental uncertainties due to flow curvature and bleed shock. Without incident shock the bleed mass flow was underpredicted by the computations over the range of plenum pressures.

Nomenclature

A = area
D = slot width
F = flow coefficient, $m_b/A_b\rho_e U_e$
m = mass flow rate
P = static pressure
P_t = total pressure
Q = discharge coefficient or sonic flow coefficient
R = gas constant
T_t = total temperature
U = velocity component in x direction
x, y = Cartesian coordinate system
α = shock generator deflection angle
γ = specific heat ratio, 1.4 for air
δ = boundary-layer thickness
ρ = density

Subscripts
b = bleed
e = outside the boundary layer
loc = local condition
plen = plenum exit
r = reference condition
1 = condition after the incident shock
∞ = freestream condition

Introduction

BLEED is used in supersonic inlets to control the effects of flow separation associated with shock boundary-layer interactions on ramps, cowls, and side walls. In order to predict the effect of bleed on the boundary-layer development and internal shock structure, few investigators[1–3] included ramp chambers, throat plenum, and exit louvers in their supersonic inlet flow simulations. However, because of the enormous increase in computational time and grid generation complexity, most investigators simulated the global effects of bleed by changing the boundary conditions[4–7] and/or the turbulence models[8,9] in the bleed regions. The imposed mass flux in the bleed area was based on experimental measurements in some investigations[7] and on empirical correlation of the bleed discharge coefficient in others.[4–6] Even when the turbulence model was modified for mass removal at the porous wall[8] the effect of bleed on boundary-layer development was not adequately predicted. In general, bleed models are restricted by the particular flow conditions and any inadequacies in the experimental data used in their model development. According to Hamed and Shang[10] the conclusions regarding the effects of bleed hole size and bleed location relative to the shock were not consistent among several experimental studies.

Edwards and McRae,[11] Hahn et al.,[12] and Hamed et al.[13,14] followed an alternative approach to investigating bleed effects. They conducted numerical simulations in which the viscous flowfield was resolved inside the individual bleed holes and slots. This approach helps in understanding the important local phenomena that control the flow in the bleed regions, and how they are affected by the bleed configuration and the external flow conditions. These types of investigations can and have been used in simple flow configurations to study the relative effects of bleed/slot angle, size, and location.

The purpose of the present numerical study is to investigate the effects of external flow and plenum conditions on bleed performance and to compare the computational results with experimental data. In the investigated configuration, bleed is applied to a flat plate turbulent boundary layer through a normal slot. The numerical solution to the viscous flow inside the slot and plenum and over the plate surface were obtained for supersonic flow with and without impinging shock at the slot's upstream corner. The flow computations were conducted over a range of plenum pressures up to choked bleed conditions. The results are compared with experimental data of Willis et al.[15] and Davis et al.[16] in terms of the flow characteristics inside the bleed slot and the variation in the bleed discharge coefficient with plenum pressure.

Presented as Paper 95-0033 at the AIAA 33rd Aerospace Sciences Meeting and Exhibit, Reno, NV, Jan. 9–12, 1995; received April 7, 1995; revision received Aug. 25, 1995; accepted for publication Sept. 4, 1995.

*Professor, Department of Aerospace Engineering and Engineering Mechanics. Fellow AIAA.

†Post-Doctoral Assistant, Department of Aerospace Engineering and Engineering Mechanics; currently Associate Professor, Department of Aeronautical Engineering, Feng Chia University, Taiwan, Republic of China. Member AIAA.

‡Graduate Research Assistant, Department of Aerospace Engineering and Engineering Mechanics. Student Member AIAA.

Flow Configuration and Computational Details

In the investigated flow configuration shown schematically in Fig. 1, bleed is applied through a normal slot to the turbulent boundary layer on a flat plate. The bleed slot, whose width is 1 cm and depth is 2.54 cm, is connected to a 41.4 × 63.5 cm plenum. Outside of the slot, the solution domain extended 12.2 cm above and 40.9 cm along the flat plate surface. The boundaries AB and CD were located at 28.2 cm upstream and 12.7 cm downstream of the slot's upstream corner to match the locations of experimental velocity profile.[15,16]

The flow computations were conducted using the PARC code[17] with the low Reynolds number k-ε turbulence model of Chien[18] modified by Nichols[19] for compressibility effects. This was based on an assessment of various algorithms and turbulence models in predicting two-dimensional shock/boundary-layer interactions with flow separation.[20] The change in bleed mass flow rate was achieved through changing the static pressure at the plenum's outflow boundary. Referring to Fig. 1, the upstream boundary conditions consisted of a boundary-layer velocity profile obtained from flat plate computations to match the experimentally measured profile's displacement and momentum thickness. All flowfield values in preshock and postshock conditions were specified along the upper boundary to locate the inviscid incident shock at the upstream corner of the slot and flat plate surface. Flow variables were extrapolated at the downstream boundary. Along the plenum's outflow boundary, the static pressure was specified to control the bleed mass flow. The initial conditions were specified from the solution without bleed for a given freestream Mach number. Subsequently, the computed flowfield with the bleed slot and plenum was used to initialize the solutions at higher bleed mass flow rates (lower plenum pressure settings).

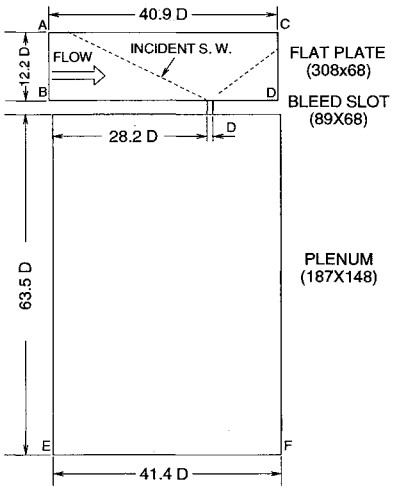

Fig. 1 Schematic of computational domain.

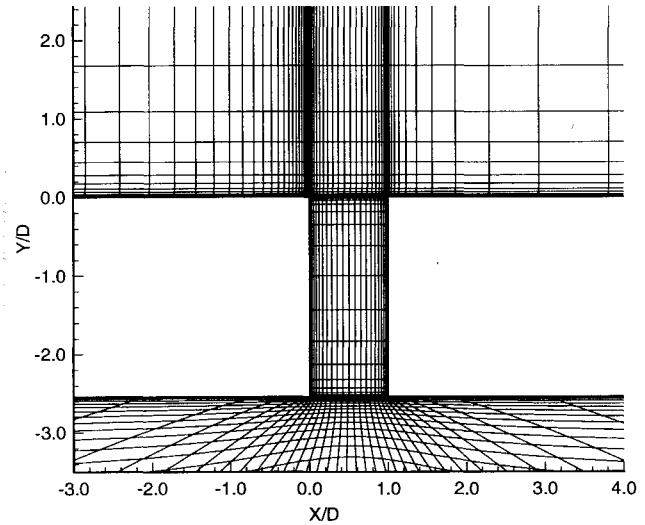

Fig. 2 Computational grid near bleed slot.

A grid independence study was conducted for the flow over flat plate with an incident shock. The grids were clustered in the y direction near the wall and in the x direction around the location of the incident shock interaction with the flat plate. Two grid systems with the same stretching factors, a (462 × 102) grid with $\Delta y_{min} = 9.738 \times 10^{-4}$ cm and $\Delta x_{min} = 2.142 \times 10^{-3}$ cm, and a (308 × 68) grid with $\Delta y_{min} = 1.497 \times 10^{-3}$ cm and $\Delta x_{min} = 3.246 \times 10^{-3}$ cm, were used to compute the flowfield at $M = 2.46$ with an incident shock whose wedge angle $\alpha = 8$ deg caused flow separation. The latter grid system could resolve the boundary-layer profiles and the flowfield with and without incident shock and the former grid showed very close boundary-layer development as the latter case in case of no shock, however, the former showed difficulties resolving the flow near the densely clustered interaction region when the incident shock was introduced. The flux error level was not decreasing, even with a quite small Courant–Friedrichs–Lewy (CFL) number of 0.2, seemingly because the fine grids near the interaction region were not capable of resolving the disturbances properly. Finally, the latter grid was chosen as a compromise to resolve the shock-induced flow separation, which already resolved the boundary layer without the incident shock. Subsequently, it was used in the discretization of the flowfield above the plate surface in the case with bleed slot and plenum.

The computational grid shown in Fig. 2 includes a 308 × 68 grid over the flat plate surface, 89 × 68 grid inside the bleed slot, and 187 × 148 grid inside the plenum chamber. Variable grid spacing was used in both x and y directions for grid clustering around the bleed walls, plenum chamber walls, and at the plate surface, with $\Delta x_{min} = 3.246 \times 10^{-3}$ cm and $\Delta y_{min} = 1.497 \times 10^{-3}$ cm corresponding to $y^+ = 2.7$ at the inflow turbulent boundary layer at 2.46 freestream Mach number. Converged steady-state solutions were obtained with a minimum CFL number of 0.2 based on six orders of magnitude reductions in the averaged rms error in the flux for all the cases without plenum. The same convergence level could not be achieved when the plenum was included in the solution domain, and had to be reduced by two orders of magnitude because of sustained flow oscillations in the plenum.

Results and Discussion

Typical results of the computed flow inside the slot near choked conditions are presented in Fig. 3 and compared with the experimental results of Davis et al.[16] reproduced in Fig. 4 for incident oblique shocks whose inviscid impact point coincides with the slot's upstream corner at $x = 0$. The figures present the pitot and static pressure contours for a shock generation angle $\alpha = 8$ deg at 2.46 freestream Mach number. The computations predict well both the shape and magnitude of the pitot pressure contours inside the slot, the location of flow separation, and the size of the separation bubbles on the slot walls. Disagreements can be observed between the experimental and computational results in a small triangular region at the slot opening upstream of the predicted bleed shock. The computed Mach number and velocity vectors, which are shown in Fig. 5, indicate flow angles of 57 deg from the slot walls in this region. This can lead to significant errors in the pitot pressure measurements, since the pitot probe was always parallel to the slot walls in the experiment. The bleed shock, which can be seen clearly in the computational results, was also not resolved by the pitot pressure measurements for the same reason. The indicated reattachment of the flow on the slot's downstream wall near the exit in the experiment was not predicted by the computations.

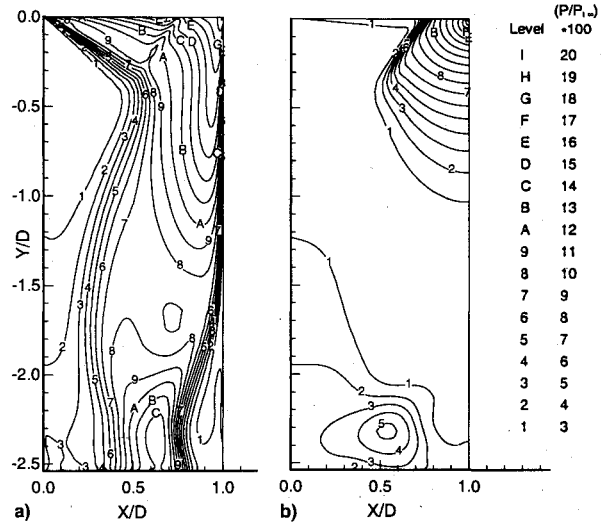

Fig. 3 Pitot and static pressure contours inside slot (computational results); $M = 2.46$, $\alpha = 8$ deg: a) pitot and b) static pressures.

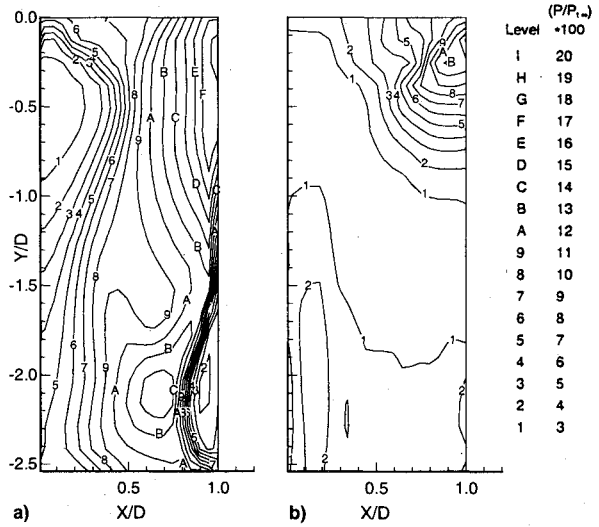

Fig. 4 Pitot and static pressure contours inside slot (experimental results[16]); $M = 2.46$, $\alpha = 8$ deg: a) pitot and b) static pressures.

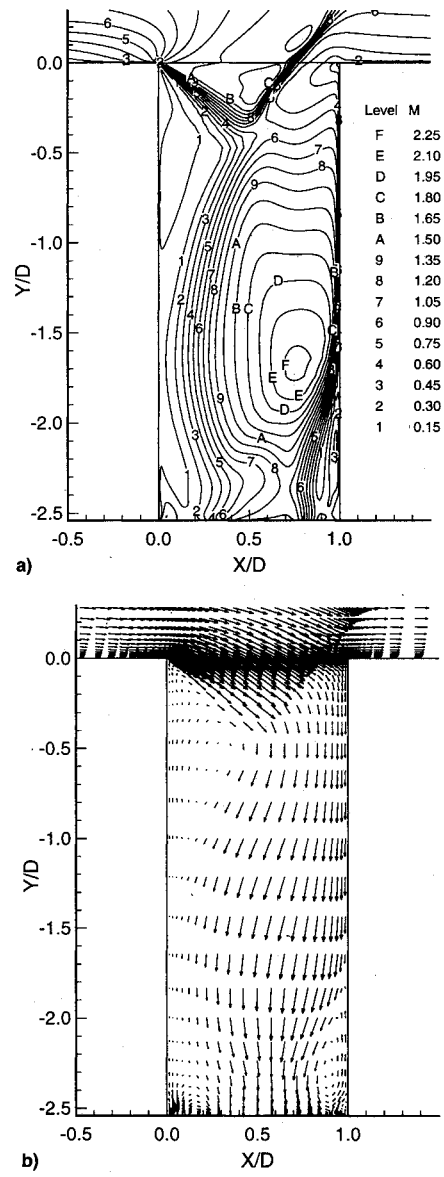

Fig. 5 Velocity field inside slot with incident shock wave; $M = 2.46$, $\alpha = 8$ deg; $P_{plen}/P_{t\infty} = 0.040$: a) Mach number contours and b) velocity vectors.

Effect of Incident Shock

The effect of the incident shock on the flow inside the slot and in the neighboring regions over the plate surface and inside the plenum is demonstrated by comparing the computational results for the Mach number and pressure contours with and without the shock (Figs. 6 and 7). The pressure contours indicate a weaker expansion fan at the slot's upstream corner when there is no incident shock. This coincides with less flow turning into the slot as can be seen from the Mach number contours. Consequently, the extent of the separated flow region along the slot's upstream walls is much larger when there is no incident shock, yielding a very limited portion of the slot opening for bleed. The ratio of the maximum computed bleed to the incoming boundary-layer mass flow was 5.1% with and 2.35% without incident shock, for the slot geometry (D/δ = 0.38). Also, without the incident shock, the bleed shock that originates inside the slot is quickly weakened outside through interactions with a second expansion fan at the slot's downstream corner.

The skin friction coefficient distribution of Fig. 8 indicates a separation bubble on the plate surface upstream of the slot in the case of incident shock. Figure 8 also indicates that there is a large difference in the predicted friction coefficients with and without incident shock within two slot widths downstream of bleed. To understand the cause of this difference, the mass flux, flow angle, and Mach number distribution across the slot opening are presented in Figs. 9–11. In the case of no incident shock, the mass flows out of the slot near the downstream slot wall in the subsonic region behind the bleed shock. This flow turns around the slot corner and forms the boundary layer over the plate surface downstream of the slot. In the case of incident shock the subsonic flow goes into the slot opening in the region behind the bleed shock and the flow over the plate surface downstream originates outside the slot.

According to the velocity profiles of Fig. 12, the effect of incident shock is seen to extend over two to three slot widths upstream and downstream of the slot, where the distorted velocity profiles are less full near the plate. The distortion upstream is associated with the shock-induced pressure gradient and flow separation. The shape of the profiles downstream is affected both by the local flow conditions above the slot and by the strength of the bleed shock at the slot opening. The bleed shock has a smaller effect on the downstream velocity profiles in the case with no incident shock because it is quickly weakened by the expansion fan at the slot's downstream corner.

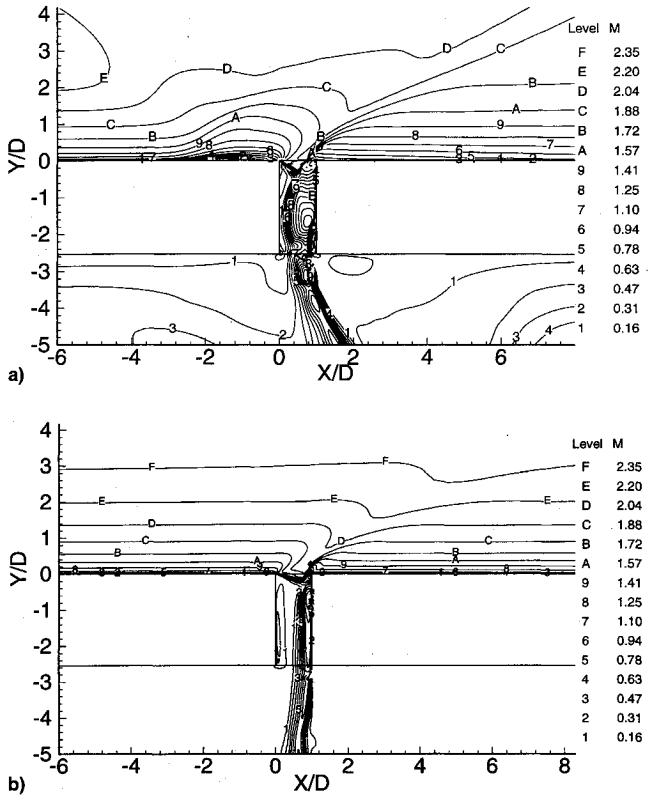

Fig. 6 Comparison of the Mach number contours: a) with incident shock ($P_{plen}/P_{t\infty}$ = 0.04) and b) without incident shock ($P_{plen}/P_{t\infty}$ = 0.032).

Discharge Coefficient

The bleed mass flow results are presented in terms of the nondimensional discharge coefficient or sonic flow coefficient[15,16] Q and the flow coefficient F:

$$Q = m_b/A_bP_r(\gamma/RT_{t\infty})^{1/2}[2/(\gamma + 1)]^{(\gamma+1)/2(\gamma-1)}$$

$$F = m_b/A_b\rho_eU_e$$

When the stagnation freestream value $P_{t\infty}$ is used for the reference pressure P_r, the discharge coefficient Q represents the ratio between the bleed mass flow and the ideal mass flow that could pass into the slot at sonic conditions if the flow was to expand isentropically to fill the bleed area A_b. On the other hand, the flow coefficient F represents the ratio between the bleed mass flow and the mass flow that would pass through the bleed area at the flow conditions outside the boundary layer.

Plenum Interactions

A considerable part of the computational effort was consumed in modeling the flowfield inside the plenum. The increased computational effort was not only associated with the number of grid points inside the plenum (50.6% of the total), but also with the predominantly low subsonic velocities in the plenum.

The bleed mass flux was monitored at both slot opening (bleed inflow) and exit (bleed outflow) during the computations. When the computations with the plenum were conducted using local time stepping, fluctuations were found to persist in the bleed mass flow at both inflow and outflow boundaries. The amplitude of the bleed mass flow fluctuations was higher at higher plenum pressures and diminished near choking. To investigate more thoroughly the nature of the bleed flow interactions with the plenum and external flowfields, one time-accurate flow simulation was performed with α = 8 deg incident shock at choked bleed conditions ($P_{plen}/P_{t\infty}$ = 0.04). The computational results indicated almost no fluctuations in the bleed mass flow at the slot's inflow boundary in this case (Table 1). An examination of the time-accurate computational results revealed that the small fluctuations in the bleed mass flow were associated with oscillations in the extent of the separated flow regions near the end walls at the slot exit. Numerical computations with local time stepping were then performed without the plenum. The bleed mass flow in these computations did not fluctuate and coincided with the time-accurate bleed mass flow at the slot's inflow boundary. One can conclude from these results that specifying the static pressure at

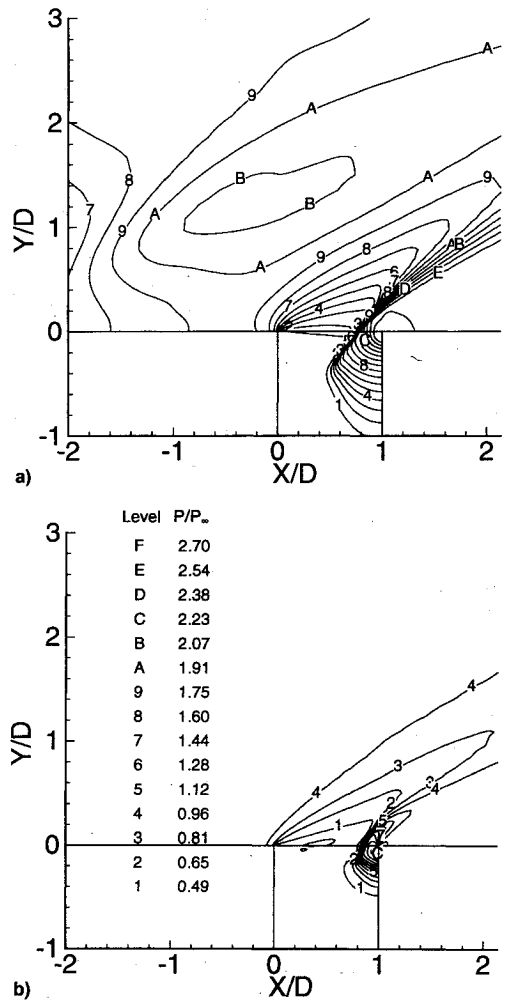

Fig. 7 Comparison of the pressure contours: a) with incident shock ($P_{plen}/P_{t\infty}$ = 0.04) and b) without incident shock ($P_{plen}/P_{t\infty}$ = 0.032).

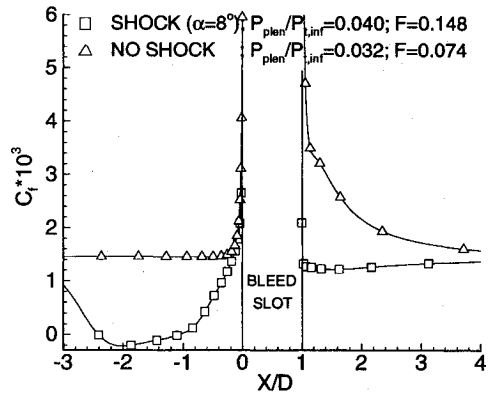

Fig. 8 Skin friction on the plate surface.

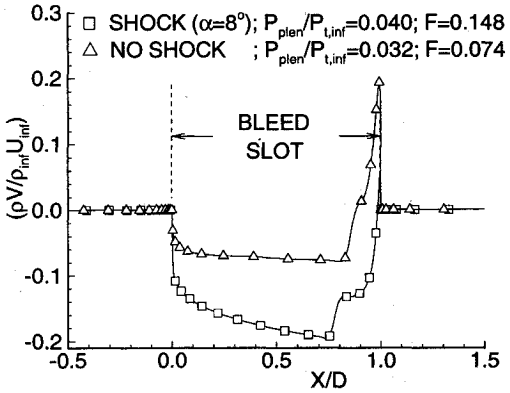

Fig. 9 Bleed mass flux across slot opening.

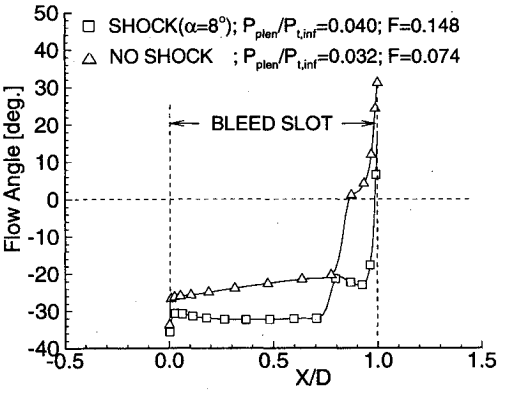

Fig. 10 Flow angle across slot opening.

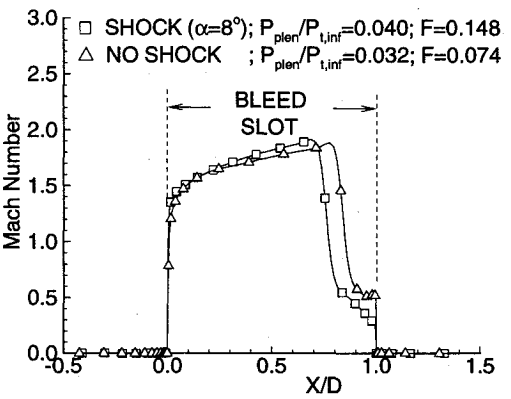

Fig. 11 Mach number across slot opening.

the bleed outflow boundary without plenum, as was done in previous studies,[13,14] is sufficient to predict the average bleed mass flow with plenum and can result in considerable reductions in CPU time.

Figure 13 shows the computed bleed mass flow without plenum as well as the range of bleed mass flow fluctuations in the computations with plenum using local time stepping. According to this figure, which also shows the experimental results of Davis et al.[16] and Willis et al.,[15] the computational results without plenum coincide with the single experimental data point with incident shock, but underpredict the bleed mass flow without shock over the range of plenum pressures. The differences can be attributed to the three-dimensional flow effects that are not modeled in the two-dimensional flow simulations. The pressure sensitive paint results presented by Davis et al. indicated three-dimensional flow effects with reduced upstream influence of the shock near the slot center, suggesting higher bleed mass flux in this region.

Table 1 Sustained bleed mass flow fluctuations at the slot opening[a]

Q	Without plenum[b]	With plenum[b]	With plenum[c]	Experiment
Mean	0.0599	0.0574	0.0604	0.0593
Maximum	0.0613	0.0609	0.0605	——
Minimum	0.0589	0.0502	0.0604	——

[a]$M = 2.46$, $\alpha = 8$ deg, $P_{plen}/P_{t\infty} = 0.040$. [b]Local time step. [c]Time accurate.

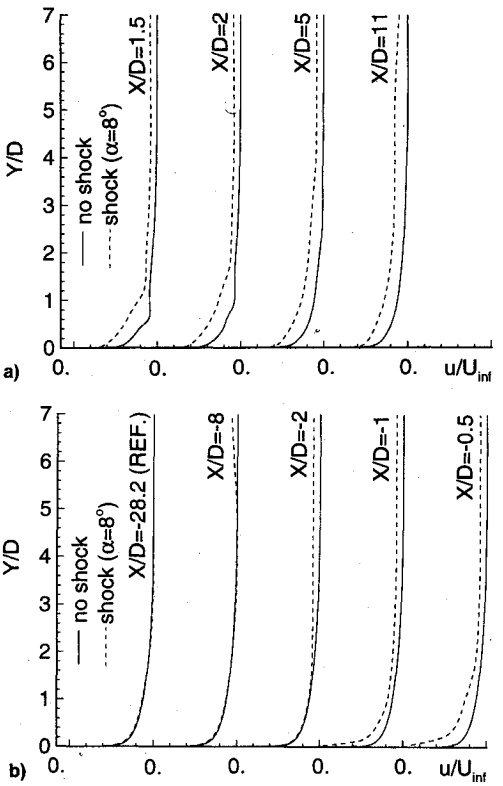

Fig. 12 Boundary-layer velocity profiles: a) upstream and b) downstream of bleed slot.

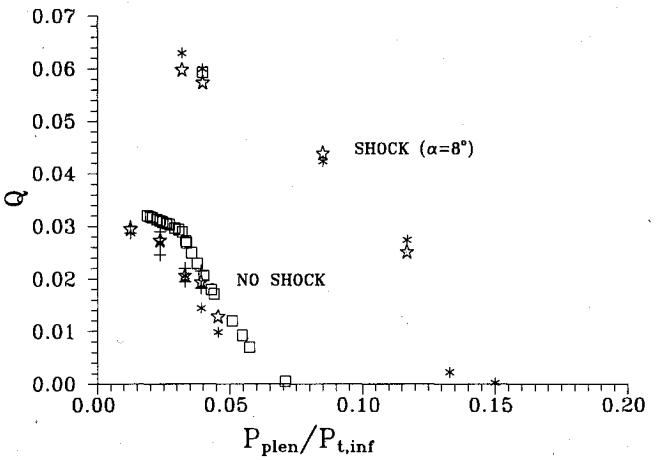

Fig. 13 Bleed discharge coefficient based on $P_{t\infty}$. □ = experimental data, * = computation without plenum, ☆ = computation with plenum, and + = range of variation with plenum.

The increase in discharge coefficient with incident oblique shock could be attributed either to the increased static pressure above the slot and/or to the distortion of the incoming boundary-layer velocity profile under the influence of the incident shock. To assess the relative effects of these two factors, a bleed discharge coefficient based on the local static pressure

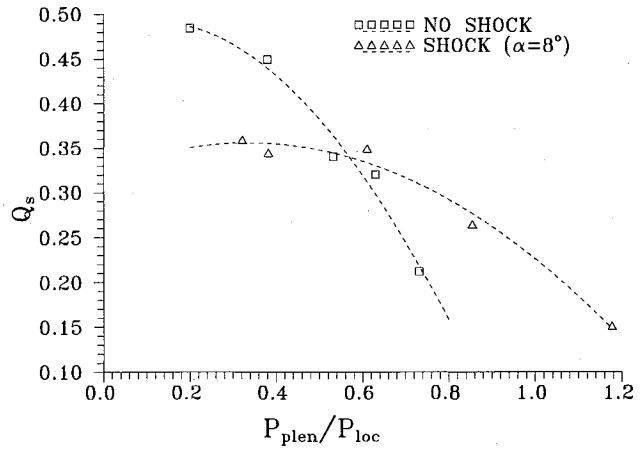

Fig. 14 Bleed discharge coefficient based on P_{loc}.

P_{loc} was used to reproduce the computed bleed results in Fig. 14. In the case of no incident shock the value of the local static pressure was taken as P_∞, whereas in the case of incident shock P_1 the inviscid static pressure behind the incident shock ($P_1/P_\infty = 1.7$) was used. One can conclude from Fig. 14 that both factors equally affect the bleed discharge coefficient.

Conclusions

Numerical simulations were conducted for supersonic flow at Mach 2.46, with bleed applied through a normal slot with and without incident shock at the slot's upstream corner. The computed results agree with the experimental measurements inside the slot in the case of incident shock. The computations indicate higher flow angles at the slot opening and a narrower separation bubble on the slot's upstream wall in the case of incident shock that leads to higher discharge coefficient. The bleed shock that originates inside the slot and extends as an oblique shock outside is quickly weakened in the case with no incident shock by the interactions with an expansion fan at the slot's downstream corner.

The plenum caused fluctuations in the bleed mass flux at the slot exit, but time-accurate computations at choked conditions indicated that these disturbances did not affect the flow and mass flux at the slot opening. The bleed mass fluctuations at the slot exit were associated with the core flow lateral movements between the two separation bubbles on the slot walls. The computed bleed mass flow without plenum coincided with the predicted steady value at the slot inlet in the time-accurate numerical simulations with plenum. The computed bleed mass flow agreed with the experimental data in the case of incident shock, but were lower with no incident shock.

Acknowledgments

This work was sponsored under NASA Grant NAG3-1213, Dave Saunders, Project Monitor. The computational work was performed on the Cray Y-MP of the Ohio Supercomputer.

References

[1]Forester, C. K., and Tjonneland, E., "New Guide for Accurate Navier-Stokes Solution of Two-Dimensional External Compression Inlet with Bleed," *16th Congress of the International Council of the Aeronautical Sciences* (Jerusalem, Israel), 1988, pp. 709–718 (ICAS 88-2.5.1).

[2]Fujimoto, A., Niwa, N., and Sawada, K., "Numerical Investigation on Supersonic Inlet with Realistic Bleed and Bypass Systems," AIAA Paper 91-0127, Jan. 1991.

[3]Fujimoto, A., and Niwa, N., "Experimental and Numerical Investigation of Mach 2.5 Supersonic Mixed Compression Inlet," AIAA Paper 93-0289, Jan. 1993.

[4]Abrahamson, K. W., "Numerical Investigation of a Mach 3.5 Axisymmetric Inlet," AIAA Paper 93-0289, Jan. 1993.

[5]Benhachmi, D., Greber, I., and Hingst, W., "Experimental and Numerical Investigation of an Oblique Shock-Wave/Turbulent Boundary Layer Interaction with Continuous Suction," AIAA Paper 89-0357, Jan. 1989.

[6]Saunders, J. D., and Keith, T. G., Jr., "Results from Computational Analysis of a Mixed Compression Supersonic Inlet," AIAA Paper 91-2581, June 1991.

[7]Reddy, D. R., Benson, T. J., and Weir, L. J., "Comparison of 3-D Viscous Flow Computations of Mach 5 Inlet with Experimental Data," AIAA Paper 90-0600, Jan. 1990.

[8]Lee, D. B., and Leblanc, R., "Interaction onde de Choc Oblique-Couch Limite sur Paroi Poreuse avec Aspiration," CP-365, AGARD, "Improvement of Aerodynamic Performance Through Boundary Layer Control and High Lift Systems," Aug. 1984 (Paper 23).

[9]Paynter, G. C., Treiber, D. A., and Knelling, W. D., "Modeling Supersonic Inlet Boundary Layer Bleed Roughness," *Journal of Propulsion and Power*, Vol. 9, No. 4, 1994, pp. 622–627.

[10]Hamed, A., and Shang, J., "Survey of Validation Data Base for Shock Wave Boundary Layer Interactions in Supersonic Inlets," *Journal of Propulsion and Power*, Vol. 7, No. 4, 1991, pp. 617–625.

[11]Edward, J., and McRae, D., "Solution Technique for Shockwave-Boundary Layer Interactions with Flow Separation and Slot Suction Effects," AIAA Paper 91-0652, Jan. 1991.

[12]Hahn, T. O., Shih, T. I-P., and Chyu, W. J., "Numerical Study of Shock-Wave/Boundary-Layer Interactions with Bleed," *AIAA Journal*, Vol. 31, No. 5, 1993, pp. 869–876.

[13]Hamed, A., Shih, S., and Yeuan, J. J., "Investigation of Shock/Turbulent Boundary-Layer Bleed Interactions," *Journal of Propulsion and Power*, Vol. 10, No. 1, 1994, pp. 79–87.

[14]Hamed, A., and Lehnig, T., "Effect of Bleed Configuration on Shock/Laminar Boundary-Layer Interactions," *Journal of Propulsion and Power*, Vol. 11, No. 1, 1995, pp. 42–48.

[15]Willis, B., Davis, D., and Hingst, W., "Flow Coefficient Behavior for Boundary-Layer Bleed Holes and Slots," AIAA Paper 95-0031, Jan. 1995.

[16]Davis, D., Willis, B., and Hingst, W., "Flowfield Measurements in Slot-Bled Oblique Shock-Wave and Turbulent Boundary-Layer Interaction," AIAA Paper 95-0032, Jan. 1995.

[17]Cooper, G. K., and Sirbaugh, J. R., "PARC Code: Theory and Usage," Arnold Engineering Development Center, AEDC-TR-89-15, Dec. 1989.

[18]Chien, K.-Y., "Prediction of Channel and Boundary-Layer Flows with a Low Reynolds Number Turbulence Model," *AIAA Journal*, Vol. 20, No. 1, 1982, pp. 33–38.

[19]Nichols, R. H., "A Two-Equation Model for Compressible Flows," AIAA Paper 90-0494, Jan. 1990.

[20]Hamed, A., "An Investigation of Oblique Shock/Boundary Layer Interaction Control," Air Force Office of Scientific Research, AFOSR Technical Rept. Contract 91-0101, Univ. of Cincinnati, Cincinnati, OH, Jan. 1992.